Acta Pharmaceutica Sinica B 2026;16(7):4692−4705

Chinese Pharmaceutical Association
Institute of Materia Medica, Chinese Academy of Medical Sciences

Acta Pharmaceutica Sinica B

www.elsevier.com/locate/apsb
www.sciencedirect.com

ORIGINAL ARTICLE

Target degradation of CASPASE-1 for alleviation of inflammation in sepsis *via* optogenetically engineered extracellular vesicles

Yuting Du[a,b,†], Dan Xiao[a,b,†], Heng Li[a,b,c,†], Li Fan[a], Kuo Shen[d], Bin Zhang[b,e], Liang Zhang[b,e], Lifei Guo[a,b], Qingzhe Li[a,b], Jinwang Zheng[a], Jingxiang Wang[a], Li Yao[f], Guodong Yang[b,*], Xuekang Yang[a,*]

[a]*Department of Burns and Cutaneous Surgery, Xijing Hospital, Air Force Medical University, Xi'an 710032, China*
[b]*The State Laboratory of Cancer Biology, Department of Biochemistry and Molecular Biology, Air Force Medical University, Xi'an 710032 China*
[c]*No. 904 Hospital of the PLA Joint Logistics Support Force, Wuxi 214000, China*
[d]*Air Force Hospital of Western Theater Command, Chengdu 500643, China*
[e]*Department of Ultrasound Medicine, Tangdu Hospital, Air Force Medical University, Xi'an 710038, China*
[f]*Department of Pathology, Xi'an No. 3 Hospital, The Affiliated Hospital of Northwest University, Xi'an 710018, China*

Received 27 August 2025; received in revised form 4 December 2025; accepted 5 December 2025

KEY WORDS

Sepsis;
Inflammation;
CASPASE-1;
Macrophage;
Lysosome-targeting;
Engineered extracellular vesicles;
Optogenetics;
Targeted protein degradation

Abstract Sepsis is a comprehensive ailment of systemic inflammatory response syndrome arising from infection. Activation of CASPASE-1 plays a central role in initiating the inflammatory cascade during sepsis. Herein, we construct optogenetically engineered extracellular vesicles (EVs) that achieve the specific degradation of CASPASE-1 and inhibit sepsis-associated inflammation. Specifically, blue light (460 nm)-induced CRY2/CIBN heterodimerization was applied during the EVs production stage to selectively load GCE−CTM fusion proteins into EVs by EXPLORs technology, yielding $EVs^{GCE-CTM}$ loading efficiency compared to conventional methods. Upon systemic delivery, $EVs^{GCE-CTM}$ preferentially accumulated in macrophages, where the GCE domain selectively bound activated CASPASE-1. The CTM motif then facilitated its lysosomal degradation by chaperone-mediated autophagy, resulting in potent inhibition of CASPASE-1 activity. In a murine model of sepsis, treatment with $EVs^{GCE-CTM}$

*Corresponding authors.
E-mail addresses: yangxuekangburns@163.com (Xuekang Yang), yanggd@fmmu.edu.cn (Guodong Yang).
[†]These authors made equal contributions to this work.

Peer review under the responsibility of Chinese Pharmaceutical Association and Institute of Materia Medica, Chinese Academy of Medical Sciences.

https://doi.org/10.1016/j.apsb.2026.05.007

effectively attenuated systemic inflammation, reduced multi-organ damage, and significantly improved survival outcomes. This approach enables highly efficient, ubiquitin-independent degradation of intracellular target proteins through macrophage-directed EVs delivery, offering a potential therapeutic approach to address sepsis and other inflammation-related diseases.

1. Introduction

Sepsis, a life-threatening systemic inflammatory storm triggered by infection, is characterized by a mortality rate exceeding 20%[1−9]. Its pathogenesis is rooted in the dysregulated CASPASE-1-mediated inflammatory cascade[10−12]. While small-molecule inhibitors and RNA-based interventions targeting CASPASE-1 have shown preclinical potential, their clinical translation remains hampered by off-target toxicity[13], delayed therapeutic efficacy, and an inability to precisely modulate post-translational modifications, underscoring the urgent need for safer and more efficient therapeutic paradigms[14].

Although proteolysis-targeting chimeras exploit ubiquitination for targeted protein degradation[15,16], current proteolysis-targeting chimeras strategies lack targeted delivery to macrophages *in vivo*[17,18]. Similarly, while extracellular vesicles (EVs) exhibit intrinsic macrophage-targeting capacity as drug carriers, conventional engineering approaches fail to achieve high-efficiency protein loading[19], let alone coordinated "target recognition−lysosomal degradation" cascades[20].

Here, we present a synergistic "optogenetically controlled assembly−lysosomal targeting" strategy by engineering EVs (EVs$^{GCE-CTM}$)[21−23]. First, EXPLORs-based optogenetic systems enable precise packaging of fusion proteins consisting of the GSDM C-terminal exosite (GCE, a CASPASE-1−recruiting domain) and a C-terminal lysosome-targeting motif (CTM)[22,24]. Second, the PTGFRN−CRY2 and CIBN−GCE−CTM photoresponsive module ensures macrophage-specific delivery and release of GCE−CTM. Third, the released GCE−CTM selectively recruits CASPASE-1 and directs its lysosomal degradation. Using a murine sepsis model induced by cecal ligation and puncture (CLP), EVs$^{GCE-CTM}$ treatment markedly decreased concentrations of IL1β and IL18 in serum, mitigated multiorgan injury, and improved survival rates. This research provides a new platform for the regulation of protein degradation therapy in inflammatory diseases.

2. Materials and methods

2.1. Cell culture and transfection

HEK293T and RAW264.7 cells were obtained from the American Type Culture Collection (ATCC, Manassas, VA, USA). HEK293T cells were maintained in Dulbecco's Modified Eagle Medium (DMEM; KeyGen Biotech, Nanjing, China) supplemented with 10% fetal bovine serum (Excell Bio, Suzhou, China) and 1% penicillin-streptomycin antibiotics (Solarbio, Beijing, China). RAW264.7 macrophages were cultured in RPMI 1640 medium (HyCyte, Suzhou, China) at 37 °C under 5% CO2. The culture medium was refreshed every other day.

For transfection, HEK293T cells were seeded at a density of 4×10^5 cells per well in a 6-well plate and transfected with plasmids using Lipofectamine 2000 (Thermo, 11668030, Shanghai, China) following the manufacturer's protocol after 24 h of incubation. The medium was then replaced with serum-free medium, and the cells were exposed to blue light for 48 h. The conditioned medium was then collected. Engineered EVs were isolated from the supernatant by ultracentrifugation. As controls, EVs^{Ctrl} were collected from plasmid-transfected cells maintained without blue-light exposure during the collection period, and EVs^{None} were collected from cells without plasmid transfection and without blue-light exposure. EVs were isolated from conditioned media by differential ultracentrifugation. Supernatants were clarified by sequential centrifugation at 4 °C (300×*g*, 10 min; 2000×*g*, 20 min; 10,000×*g*, 30 min, using a Centrifuge 5424 R, Eppendorf, Hamburg, Germany) and passage through a 0.22-μm sterile filter (Merck Millipore, Burlington, MA, USA). Vesicles were collected by ultracentrifugation (Beckman Coulter, A94516, Brea, CA, USA) at 110,000×*g* for 70 min at 4 °C. The pellet was washed in excess sterile water (in-house prepared) and re-pelleted under the same conditions. Final pellets were resuspended in 100 μL PBS (Thermo, 10010023, Shanghai, China), aliquoted, and stored at −80 °C.

2.2. Plasmid construction

Nanjing GenScript Biotech Corporation (Nanjing, China) used the pcDNA3.1(−) plasmid to clone and synthesize the recombinant genes *Ptgfrn-CRY2* and *CIBN-Gce-Ctm*.

2.3. EVs characterization and labeling

In brief, EVs were deposited onto a metal grid and subsequently stained with 2% uranyl acetate (Electron Microscopy Sciences, Hatfield, PA, USA). After drying for 30 min, the EVs were visualized using a transmission electron microscope (JEOL Ltd., JEM-1400Flash, Tokyo, Japan). For the analysis of EVs distribution, the isolated EVs were uniformly diluted to a protein concentration of 500 ng/mL and examined using a Zeta View system (Particle Metrix, PMX 110, Meerbusch, Germany).

2.4. Enzyme-linked immunosorbent assays

The concentrations of IL1β and IL18 in cell culture supernatants and mouse serum were quantified using commercial mouse-specific ELISA kits (for IL1β, EK201B; for IL18, EK218; both from MultiSciences (Lianke) Biotech Co., Ltd., Hangzhou, China) according to the manufacturer's instructions.

2.5. Western blot

Proteins were isolated from cells, tissues, and EVs using RIPA lysis buffer (Beyotime, Shanghai, China), and their concentrations were determined by the Pierce BCA Protein Assay Kit (Thermo, 23225, Shanghai, China). Samples were separated by sodium dodecyl sulfate-polyacrylamide gel electrophoresis and subsequently transferred onto nitrocellulose membranes (Merck Millipore, HATF00010, Burlington, MA, USA). The membranes were then blocked with 5% nonfat milk for 1 h, followed by overnight incubation with primary antibodies: anti-GAPDH (Proteintech, 10494-1-AP, Wuhan, China), anti-GM130 (Proteintech, 11308-1-AP, Wuhan, China), anti-CD9 (Affinity Biosciences, AF5139, Liyang, China), anti-TSG101 (Proteintech, 28283-1-AP, Wuhan, China), anti-IL18 (Abcam, AB207323, Cambridge, UK), anti-CASPASE-1 (Proteintech, 22915-1-AP, Wuhan, China), anti-Cleaved CASPASE-1 (Cell Signaling Technology, #67314, Boston, MA, USA), anti-IL1β (Cell Signaling Technology, #31202, Danvers, MA, USA), anti-NLRP3 (Proteintech, 30109-1-AP, Wuhan, China), and anti-Flag (Proteintech, 66008-4-Ig, Wuhan, China). Following three washes with TBST (in-house prepared: 20 mmol/L Tris-HCl, 150 mmol/L NaCl, 0.1% Tween-20, pH 7.6), the membranes were exposed to HRP-conjugated secondary antibodies (Abcam, ab6721, Cambridge, UK) at room temperature for 1 h, and the protein bands were detected using ECL substrate (Thermo, 32106, Shanghai, China). Data from Western blots were normalized to GAPDH and are presented as relative levels compared to the control group (set to 1). Data are presented as the mean $\pm$ standard error of mean (SEM) of three independent experiments. Statistical significance was determined by one-way analysis of variance (ANOVA) with Tukey's *post hoc* test (ns, not significant; $^{*}P < 0.05$, $^{**}P < 0.01$, $^{***}P < 0.001$).

2.6. Quantitative real-time polymerase chain reaction (qRT-PCR)

Total RNA was extracted using TRIzol reagent (Invitrogen, 15596026CN, Carlsbad, CA, USA) following the manufacturer's protocol. Reverse transcription was carried out using a Prime Script First-Strand cDNA Synthesis Kit (Roche, 04897030001, Basel, Switzerland). qPCR reactions were conducted with FastStart Essential DNA Green Master (Roche, 06402712001, Basel, Switzerland). Each PCR reaction was performed in triplicate. Data acquisition and analysis were conducted using a Roche Light Cycler 96 qPCR system (Roche, LightCycler 96, Basel, Switzerland). Expression was normalized to *Gapdh*, and fold changes were calculated by the $2^{-\Delta\Delta Ct}$ method.

2.7. Mice

All experimental procedures were executed according to the protocols approved by the Animal Care and Use Committee of the Fourth Military Medical University. We used male C57BL/6 mice that were 8−10 weeks old and weighed 22−25 g. All experiments were authorized by the Animal Care and Use Committee of the Fourth Military Medical University (Approval No. KY20213144-1).

2.8. High-grade CLP sepsis model and treatment regimen

The high-grade sepsis model was executed as described (Supporting Information Fig. S1). Mice were anesthetized *via* intraperitoneal injection of 1% pentobarbital sodium (Sigma−Aldrich, St. Louis, MO, USA) before all procedures. Following anesthesia, the peritoneum was surgically exposed under sterile conditions. About 75% of the cecum was securely tied with a 4-0 silk suture (Ethicon, Somerville, NJ, USA), followed by a single perforation made using a 21-gauge needle (BD, Franklin Lakes, NJ, USA). To ensure proper patency, a small amount of fecal material was extruded from the perforation site. The cecum was then placed back into the peritoneal cavity, and the abdominal wound was sutured with 4-0 silk suture. Immediately post-CLP, the animals received subcutaneous pre-warmed saline (50 ml/kg) for fluid resuscitation. In the sham-operated group, mice underwent identical surgical procedures without cecal ligation and perforation.

2.9. In vivo biodistribution of EVs

EVs were labeled with 1,1′-dioctadecyl-3,3,3′,3′-tetramethylindotricarbocyanine iodide (DiR; Invitrogen, D12731, Carlsbad, CA, USA) at a final dye concentration of 8 μmol/L. Unincorporated dye was removed by size-exclusion chromatography, and labeled EVs were washed three times in PBS before intravenous injection (tail vein; 100 μL; dose specified). *In vivo* fluorescence imaging was performed 6 h post-injection under isoflurane (YaJi Biological, YS1414M, Shanghai, China) anesthesia using an IVIS Lumina II system (PerkinElmer, Waltham, MA, USA) with 745/800 nm (Ex/Em) filters (Fig. S1). The 6-h time point was selected based on preliminary kinetics showing the highest target-to-background ratio. Tissues (heart, liver, spleen, lung, and kidney) were harvested at 6 h for *ex vivo* imaging.

For cellular uptake analysis, tissue sections from mice receiving Dil-labeled (Invitrogen, D282, Carlsbad, CA, USA) EVs were fixed, blocked with 5% BSA (Sigma−Aldrich, A7906), and permeabilized as needed, followed by incubation with anti-F4/80 (Abcam, EPR26545-166, Cambridge, UK; 1 h at room temperature; appropriate dilution) and a fluorophore-conjugated secondary antibody. Nuclei were counterstained with Hoechst (Beyotime, C1029, Shanghai, China). Images were acquired on a Nikon A1 Spectral Confocal Microscope (Nikon, Tokyo, Japan).

2.10. Histopathologic assessment

Tissues such as the heart, liver, lung, spleen, and kidney were collected and preserved in 4% buffered formaldehyde (Sigma−Aldrich, 100496). They were then embedded in paraffin (Sigma−Aldrich, P3558) and serially sectioned (4 μmol/L). Each slide was stained with hematoxylin and eosin (Sigma−Aldrich, HHS16). Morphological damage was examined microscopically.

2.11. Flow cytometry

Pyroptosis in treated and untreated cells was assessed by flow cytometry with propidium iodide (PI; Sigma-Aldrich, P4170) and CASPASE-1 (Abcam, ab219935, Cambridge, UK) staining. Cells were collected by centrifugation at 200×*g* (Eppendorf) for 5 min after two PBS washes, then incubated with CASPASE-1 antibody and PI for 1 h at room temperature in the dark. Flow cytometric analysis was performed, and experiments were conducted at least three times.

2.12. Hemolysis assay

Hemocompatibility of the EVs$^{GCE-CTM}$ was assessed by a standard hemolysis assay. Fresh whole blood from healthy C57BL/6 mice was collected in heparinized tubes (BD, 367874, Franklin Lakes, NJ, USA). Red blood cells were isolated by centrifugation at 1000×*g* (Eppendorf) for 10 min at 4 °C and washed three times with PBS until the supernatant was clear. Purified RBCs were resuspended in PBS to obtain a 2% (*v*/*v*) RBC suspension.

Aliquots of the 2% RBC suspension were incubated with EVs, PBS, and deionized water at 37 °C for 2 h. PBS and deionized water served as the negative (0% hemolysis) and positive (100% hemolysis) controls, respectively. After incubation, samples were centrifuged at 1000×*g* (Eppendorf) for 10 min, the supernatants were transferred to a 96-well plate, and absorbance was recorded at 540 nm using a microplate reader (BioTek Instruments, Synergy H1, Winooski, VT, USA). Hemolysis was calculated as the following Eq. (1):

$$\text{Hemolysis}\,(\%) = [(A_{\text{sample}} - A_{\text{PBS}}) / (A_{\text{deionized water}} - A_{\text{PBS}})] \times 100 \quad (1)$$

where A_{sample}, A_{PBS}, and $A_{\text{deionized water}}$ are the absorbances of the sample, negative control (PBS), and positive control (deionized water), respectively.

2.13. Echocardiography

Fur from the chest to the abdomen was removed with a chemical depilatory. Mice were placed on a temperature-controlled warming pad and anesthetized with isoflurane (YaJi Biological). Transthoracic echocardiograms were acquired using a Vevo 2100 system (FUJIFILM VisualSonics, Toronto, Canada). Cardiac function was evaluated with M-mode imaging and pulsed-wave Doppler of mitral inflow; systolic performance was reported as left ventricular ejection fraction, and diastolic function as the *E*/*A* ratio.

2.14. Statistical analysis

Data were analyzed with GraphPad Prism 6.02 software (GraphPad Software, San Diego, CA, USA). Student's *t*-test was used for two-group comparisons, and one-way ANOVA with Tukey's *post hoc* test was used for comparison among three or more groups. Data are expressed as mean ± SEM. Statistical significance was set at $P < 0.05$.

3. Results

3.1. Characterization and analysis of EVs$^{GCE-CTM}$

Built on the EXPLORs optogenetic platform, our system achieves precise control through three core components[21]. PTGFRN serves as a stable scaffold on the EVs membrane; CRY2, a blue-light-responsive photoreceptor, is fused to PTGFRN to create a membrane-anchored capture module; and CIBN acts as the high-affinity binding partner of CRY2[25]. In this design, CIBN is fused to a chimeric protein containing the GCE and CTM domains: GCE recruits activated CASPASE-1, while CTM targets proteins to lysosomal degradation *via* chaperone-mediated autophagy[22,23]. Upon blue-light illumination, CRY2 engages CIBN to form a molecular bridge, enabling efficient, controllable loading of the therapeutic cargo onto the EVs' surface[24]. After delivery to macrophages, the released GCE−CTM module recruits activated CASPASE-1 through GCE and directs the complex to lysosomes for degradation *via* the CTM motif. To generate EVs incorporating this construct, two plasmids were designed (Supporting Information Fig. S2). HEK293T cells were transfected with the two plasmids, resulting in the expression of the PTGFRN−CRY2 (Fig. 1A, top) and CIBN−GCE−CTM (Fig. 1A, bottom). Culture media from these transfected cells were collected, and EVs were subsequently isolated by ultracentrifugation (Fig. 1B). To confirm the identity of the isolated vesicles, Western blot analysis was performed targeting well-established EVs markers CD9 and TSG101. Both proteins were readily detected in the preparations, while the Golgi marker GM130 was absent, thus verifying the purity and EV nature of the isolates (Supporting Information Fig. S3). Additionally, we confirmed the successful expression of both fusion constructs in EVs, with CIBN−GCE−CTM and PTGFRN−CRY2, respectively, in Western blot assays of EVs lysates from transfected HEK293T cells (Fig. 1C). Quantitative analysis further demonstrated that, relative to control groups, transfected cells and their corresponding EVs exhibited elevated expression of FLAG-tagged proteins and CRY2 (Fig. 1D−G). Western blotting revealed a marked increase in FLAG expression in EVs$^{GCE-CTM}$ compared to EVs^{Ctrl} (Fig. 1H), and consistently higher levels of both FLAG and CRY2 were observed in EVs$^{GCE-CTM}$ relative to EVs^{None} and EVs^{Ctrl} (Fig. 1I). Nanoparticle tracking analysis indicated that over 80% of the isolated vesicles fell within the 30−120 nm size range (mean diameter: ∼90 nm), in line with the typical size distribution of EVs (Fig. 1J−L). Transmission electron microscopy displayed typical cup-shaped membrane vesicles, thereby confirming their identification as EVs (Fig. 1M−O).

3.2. Lysosomal targeting capacity and CASPASE-1 interaction of EVs$^{GCE-CTM}$

To investigate the intracellular fate of EVs$^{GCE-CTM}$ cargo, both the lysosomal targeting capability and CASPASE-1 binding properties of the delivered fusion proteins were assessed. Two groups of EVs were prepared following transfection: (1) non-illuminated controls (EVs$^{Light\ off}$) and (2) EVs generated under 460-nm blue light exposure for 48 h (EVs$^{GCE-CTM}$). Quantitative PCR analysis showed a significant increase in FLAG transcript levels in the illuminated group (Supporting Information Fig. S4), indicating that the EXPLORs system markedly enhances the efficiency of protein loading into EVs during their biogenesis. To assess whether the engineering modifications affected the ability of EVs to be internalized and trafficked to lysosomes by macrophages, EVs$^{GCE-CTM}$, EVs^{None}, and EVs^{Ctrl} were co-incubated with RAW264.7 macrophages. EVs were labeled with the green fluorescent dye DiO, and lysosomes were stained using LysoTracker, enabling visualization of their intracellular localization (Supporting Information Fig. S5).

We next examined whether EVs$^{GCE-CTM}$ effectively mediates lysosomal degradation of CASPASE-1 *via* GCE−CTM interaction. To mimic inflammatory conditions associated with sepsis, RAW264.7 macrophages were stimulated with lipopolysaccharide (LPS, 1 μg/mL) for 12 h[26], followed by co-incubation with either EVs$^{GCE-CTM}$ or EVs^{None}. Immunofluorescence imaging was performed to determine subcellular localization: CASPASE-1 was labeled with green fluorescence, lysosomes were stained with LysoTracker, and nuclei were counterstained with Hoechst

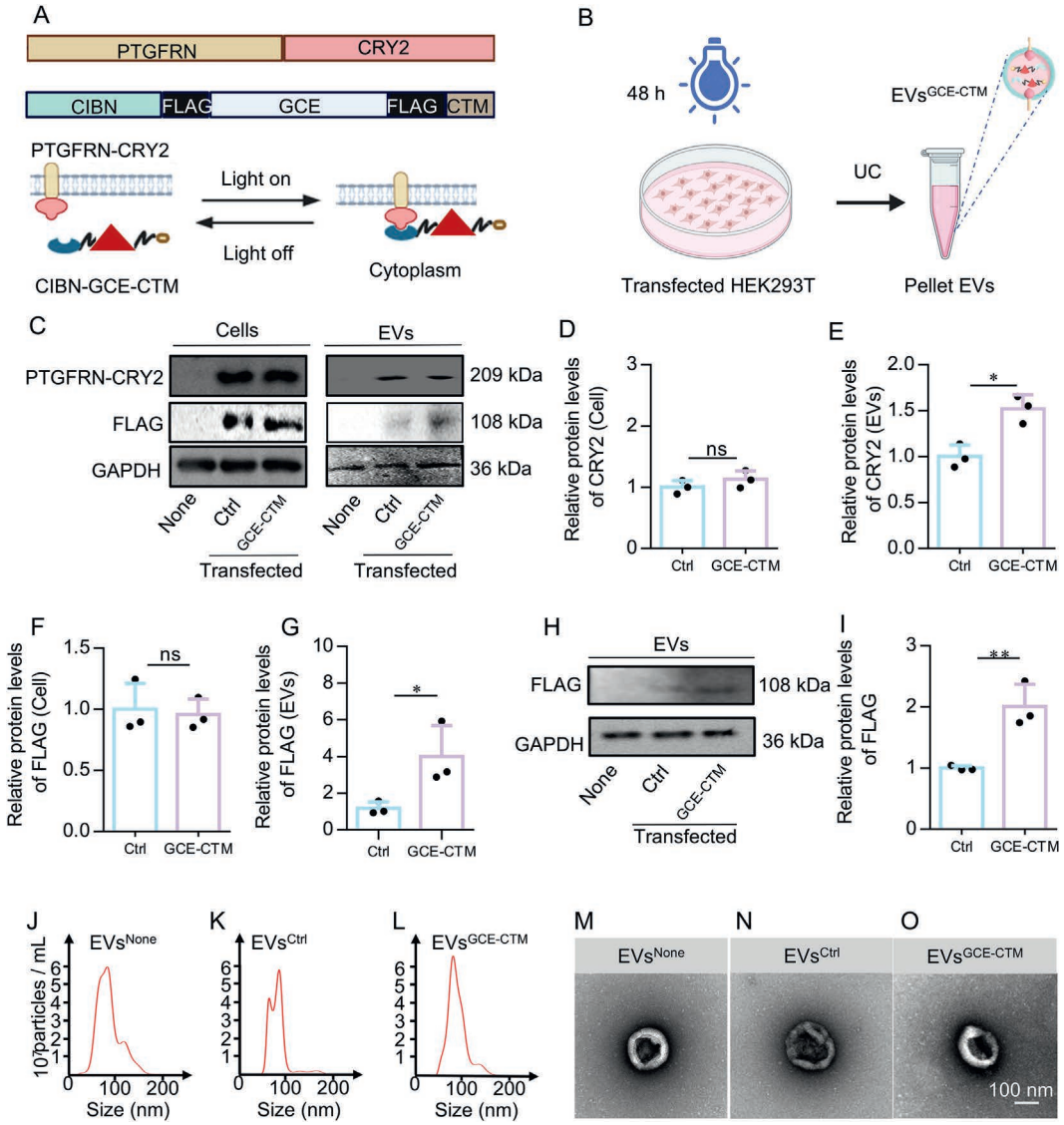

Figure 1 Preparation and characterization of EVs$^{GCE-CTM}$. (A) Schematic of DNA constructs used for the production of EVs$^{GCE-CTM}$ (top). Schematic showing fusion proteins and their proposed activities (bottom). Image created with Biorender.com, with permission. (B)Schematic diagram of the EVs preparation and isolation process. Image created with Biorender.com, with permission. (C) Western blotting analysis of CRY2 and FLAG stably expressed in transfected HEK293T cells and isolated EVs$^{GCE-CTM}$. (D–G) Quantification of protein levels. Data are presented as mean ± SEM ($n = 3$). ns, not significant; *$P < 0.05$ by Student's t-test. (H) Western blot analysis of FLAG expression in different EVs. (I) Quantification of protein levels. Data are presented as mean ± SEM ($n = 3$). **$P < 0.01$ by Student's t-test. (J–L) Size distribution of isolated EVs as indicated. Scale bar: 100 nm. EVs^{None}: These EVs were obtained from HEK293T cell culture media without transfection (Fetal bovine serum without EVs); EVs^{Ctrl}: These EVs were transfected with CIBN–GCE–CTM and PTGFRN–CRY2 without the blue light exposure. GAPDH served as the loading control.

(Fig. 2A–C). As expected, EVs$^{GCE-CTM}$ treatment led to clear colocalization of CASPASE-1 with lysosomal compartments, suggesting targeted delivery for degradation. To further validate the interaction between CASPASE-1 and the CIBN–GCE–CTM fusion protein, co-immunoprecipitation assays were performed (Fig. 2D). Immunoprecipitation using anti-FLAG magnetic beads successfully pulled down CASPASE-1, as confirmed by distinct electrophoretic bands corresponding to both CASPASE-1 and CIBN-3 × FLAG-GCE (Fig. 2E–G). These results indicate a specific molecular interaction between the fusion construct and CASPASE-1. Additional support was provided by immunohistochemistry and lysosomal co-localization analyses. Collectively, these results demonstrate that EVs$^{GCE-CTM}$ not only recruits CASPASE-1 but also directs it to lysosomes for degradation, thereby establishing the functional efficacy of the fusion protein in mediating selective protein targeting within macrophages.

To evaluate the anti-inflammatory efficacy of EVs$^{GCE-CTM}$, we examined its modulatory effects in LPS-stimulated RAW264.7 macrophages. This approach aligns with the canonical CASPASE-1 activation pathway, in which inflammasome assembly leads to autocatalytic cleavage of Pro-CASPASE-1 into the active p20 fragment. The active CASPASE-1 subsequently mediates the maturation of pro-IL1β and pro-IL18 into their respective biologically active forms[27,28]. Accordingly, we assessed the

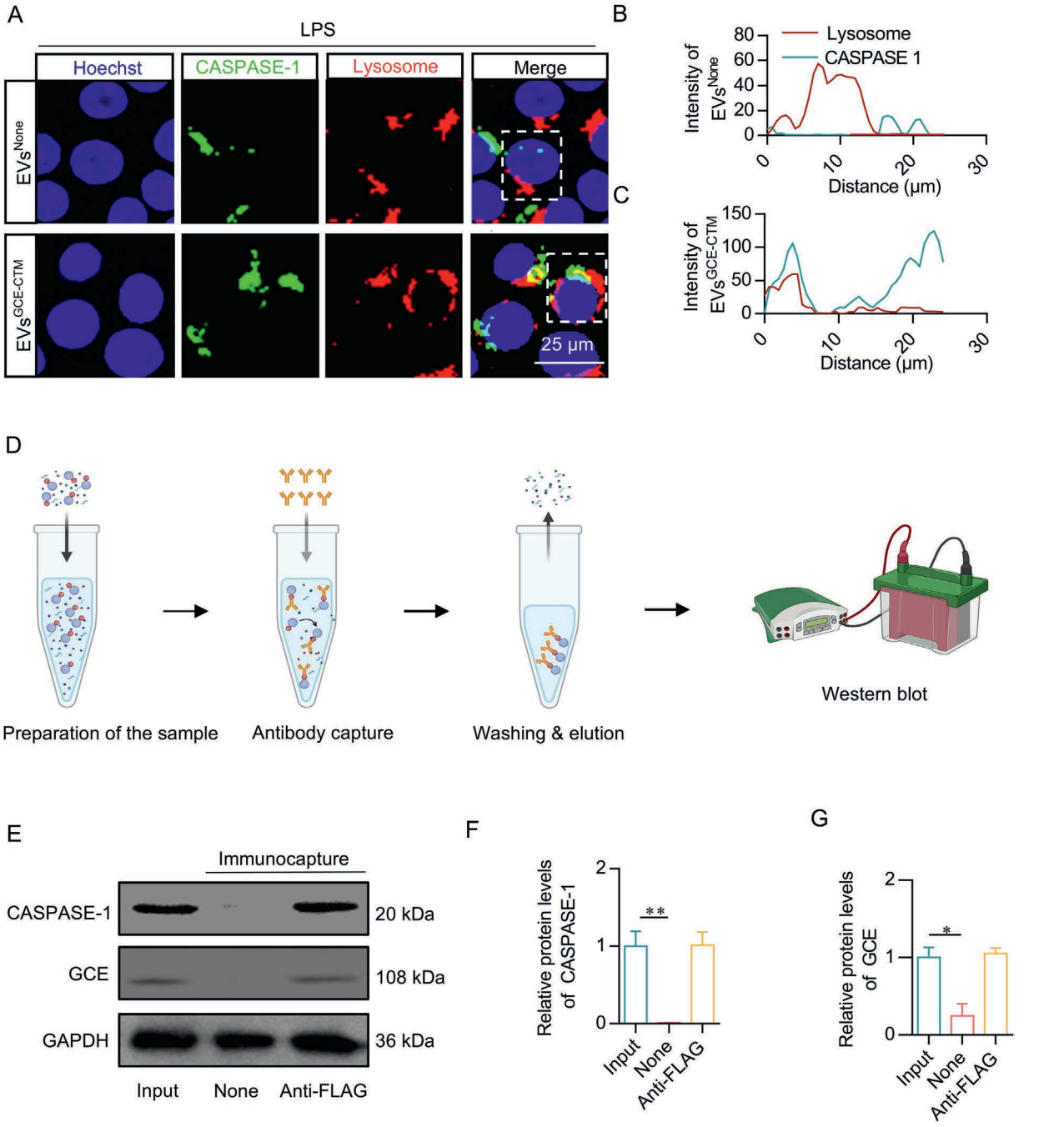

Figure 2 EVs$^{GCE-CTM}$ is targeted towards the lysosome for the degradation of CASPASE-1 in RAW264.7 cells. (A) Representative fluorescence microscopy images showing CASPASE-1 localization into lysosomes for degradation in RAW264.7 cells. EVs^{Ctrl} served as the negative control. Scale bar: 25 μm. (B, C) Quantification of fluorescence intensity. (D) Schematic of co-immunoprecipitation. Image created with Biorender.com, with permission. (E) RAW264.7 cells treated with LPS were co-cultured with EVs$^{GCE-CTM}$, followed by incubation with control or anti-FLAG magnetic beads. The immunoprecipitated complexes were lysed, and the expression levels of CASPASE-1 and the CIBN−3X-FLAG−GCE−3XFLAG−CTM fusion protein were analyzed by Western blot. (F, G) Quantification of protein levels. Data are presented as the mean ± SEM ($n = 3$). Statistical significance was determined by one-way ANOVA with Tukey's *post hoc* test (*$P < 0.05$, **$P < 0.01$).

expression levels of key components involved in inflammasome signaling, including CASPASE-1, IL1β, IL18, NLRP3, and GSDMD (Fig. 3A−E; Supporting Information Fig. S6B, S6D−S6F). Microscopic analysis revealed characteristic morphological features of pyroptosis in LPS-treated macrophages (Fig. S6A). Additionally, a lactate dehydrogenase (LDH) release assay demonstrated increased extracellular LDH activity following pyroptotic cell death[29], further confirming membrane rupture and cytolysis (Fig. S6C). To quantify cytokine secretion, the enzyme-linked immunosorbent assay (ELISA) was performed. The results revealed a marked reduction in IL18 (Fig. 3F) and IL1β (Fig. 3G) secretion in the EVs$^{GCE-CTM}$-treated group

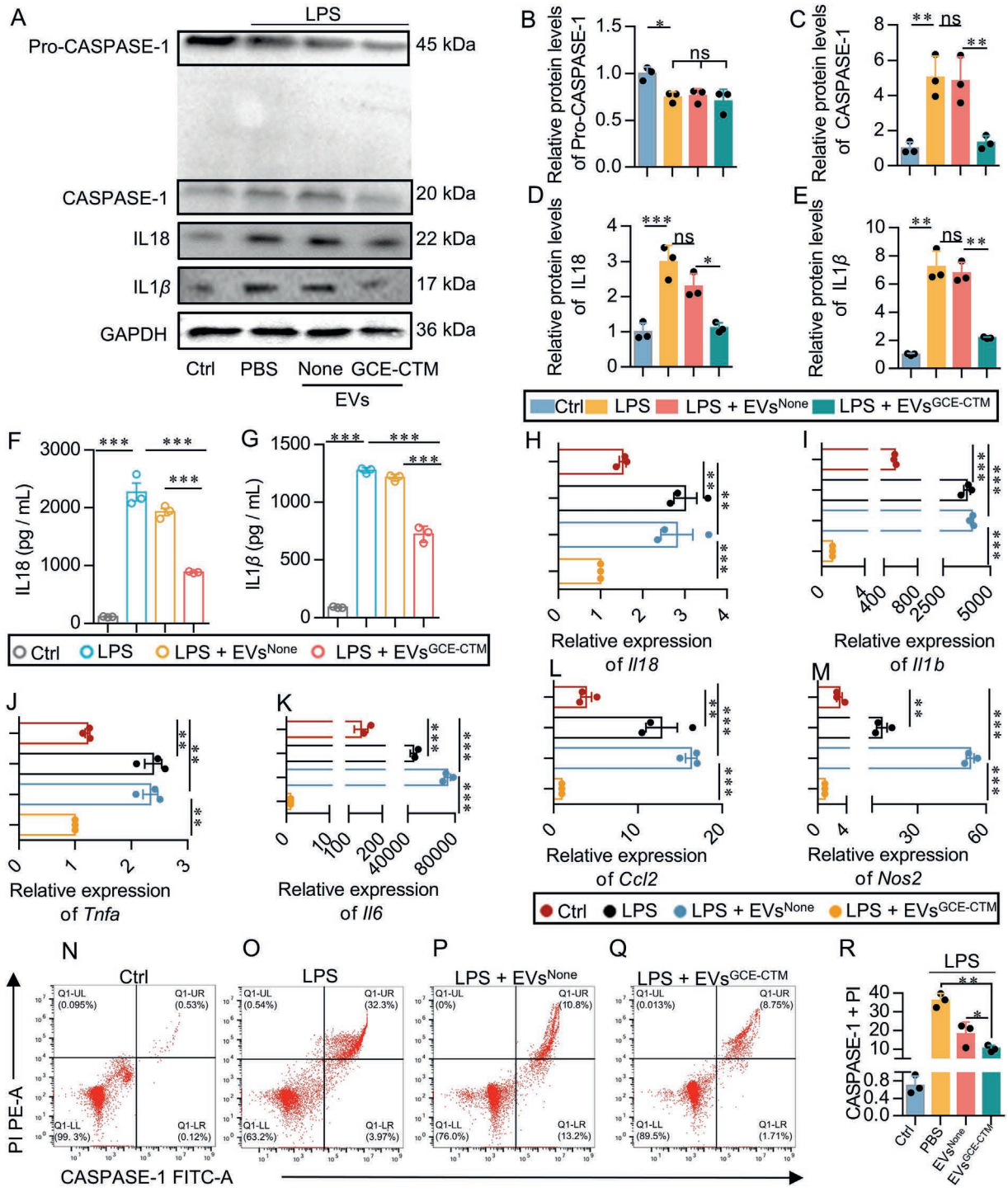

Figure 3 Degradation of CASPASE-1 and Inhibition of Inflammation by $EVs^{GCE-CTM}$ in RAW264.7. (A) Western blot analysis of the expression of Pro-CASPASE-1, cleaved CASPASE-1, IL18, and IL1β. (B−E) The quantification of protein levels. Data are presented as the mean ± SEM ($n = 3$). Statistical significance was determined by one-way ANOVA with Tukey's *post hoc* test (ns, not significant; $^{*}P < 0.05$, $^{**}P < 0.01$, $^{***}P < 0.001$). (F, G) ELISA measurement of IL18 and IL1β protein concentrations in the supernatant of RAW264.7 cells. Data are presented as the mean ± SEM ($n = 3$). Statistical significance was determined by one-way ANOVA with Tukey's *post hoc* test ($^{***}P < 0.001$). (H−M) qPCR analysis of *Il18*, *Il1b*, *Tnfa*, *Il6*, *Ccl2*, and *Nos2* in RAW264.7 cells. GAPDH was used as the loading control. Data are presented as the mean ± SEM ($n = 3$). Statistical significance was determined by one-way ANOVA with Tukey's *post hoc* test ($^{**}P < 0.01$, $^{***}P < 0.001$). (N−R) CASPASE-1+PI levels were increased after LPS treatment. Data are presented as the mean ± SEM ($n = 3$). Statistical significance was determined by one-way ANOVA with Tukey's *post hoc* test ($^{*}P < 0.05$, $^{**}P < 0.01$).

compared to LPS controls. This suppression was further corroborated at the transcriptional level *via* qPCR, which showed downregulation of multiple pro-inflammatory genes, including *Il18*, *Il1b*, *Tnfa*, *Il6*, and *Ccl2* (Fig. 3H−M), indicating effective inhibition of inflammatory signaling cascades at both post-translational and gene expression levels.

These findings collectively support the notion that EVs$^{GCE-CTM}$ promotes compartmentalized degradation of activated CASPASE-1, thereby attenuating inflammatory responses in macrophages. Consistently, flow cytometry analysis indicated elevated levels of CASPASE-1 and PI double-positive cells following LPS stimulation (Fig. 3N−Q), confirming pyroptotic activation under septic conditions. Notably, treatment with EVs$^{GCE-CTM}$ significantly reduced the proportion of CASPASE-1 and PI double-positive cells, indicating an effective attenuation of pyroptosis in macrophages (Fig. 3R).

3.3. Local inflammation alleviation by EVs$^{GCE-CTM}$ in CLP-induced septic mice

To evaluate the therapeutic potential of EVs$^{GCE-CTM}$ *in vivo*, we utilized a CLP model of polymicrobial sepsis[26,30]. DiR-labeled EVs were intravenously administered, and real-time tracking was conducted using an IVIS-based spectral imaging system in both sham-operated and CLP-treated mice (Fig. 4A). The biodistribution revealed pronounced accumulation of EVs in the liver, lung, and spleen—organs known for their central role in EVs clearance and commonly affected in sepsis-induced multiple organ dysfunction syndrome[6]. Importantly, septic mice demonstrated additional EV deposition in the heart and kidney, suggestive of increased EV uptake in extrahepatic tissues during systemic inflammation (Fig. 4B, Supporting Information Fig. S7A−S7C). To assess macrophage uptake of EVs at the tissue level, Dil-labeled EVs were injected *via* the tail vein. Harvested organs—including the heart, liver, spleen, lung, and kidney—were analyzed by fluorescence microscopy. Co-localization of Dil-labeled EVs with the macrophage marker F4/80 confirmed efficient uptake in inflamed tissues (Fig. 4C, E−I). Furthermore, intracellular tracking demonstrated CASPASE-1 translocation into lysosomes in these macrophages, indicating lysosomal degradation following EVs delivery (Fig. 4D, J−N). These findings underscore the capacity of macrophages to internalize EVs$^{GCE-C™}$ under septic conditions and facilitate targeted CASPASE-1 degradation.

3.4. EVs$^{GCE-C™}$ demonstrates the effect on sepsis in the murine model

The therapeutic efficacy of EVs$^{GCE-CTM}$ was further investigated in CLP-induced septic mice, treated with PBS, EVs^{None}, or EVs$^{GCE-CTM}$. CLP surgery involving 75% cecal ligation was used to model severe intra-abdominal sepsis (Fig. S1). Given the role of CASPASE-1 in promoting IL1β and IL18 maturation[31], we conducted Western blot analyses to examine the expression levels of cleaved CASPASE-1, IL1β, and IL18 proteins in multiple organs, including the liver, lung, spleen, kidney, and heart. The results showed that EVs$^{GCE-CTM}$ treatment markedly decreased the expression of these key inflammatory mediators compared to both the CLP and EVs^{None} groups (Fig. 5A−J; Supporting Information Figs. S8−S10). This effect was consistently observed across all examined organs, suggesting that the anti-inflammatory action of EVs$^{GCE-CTM}$ is systemic rather than tissue-specific. In addition to the reduction of pro-inflammatory cytokines, we further assessed the expression of pyroptosis and inflammasome activation markers, including GSDMD, N-GSDMD, and NLRP3. As shown in the supplementary figures (Supporting Information Figs. S11−S15), EVs$^{GCE-CTM}$ administration resulted in a significant downregulation of these markers in septic mice. These findings collectively demonstrate that EVs$^{GCE-CTM}$ effectively suppresses the execution of pyroptosis in various organs under septic conditions. Moreover, the quantification of Western blot bands revealed statistically significant differences among the three groups, further confirming the robust inhibitory effect of EVs$^{GCE-CTM}$ on inflammasome activation and pyroptosis at the protein level. These comprehensive results highlight the widespread therapeutic benefits of EVs$^{GCE-CTM}$ in mitigating systemic inflammation and organ injury in sepsis. Consistent with the protein-level findings, qPCR analysis was conducted across multiple organs—including the heart, liver, spleen, lung, and kidney—to assess transcriptional changes in key inflammatory cytokines. Results demonstrated a significant downregulation of *Il1b* and *Il1*8 mRNA levels in all examined tissues of EVs$^{GCE-CTM}$–treated mice when compared to both the CLP and EVs^{None} groups (Fig. 5K−O and Fig. 5Q−U). This widespread suppression was not limited to *Il18* and *Il1b*; additional inflammatory mediators such as *Il6*, *Tnfa*, *Ccl2*, and *Nos2* also showed markedly decreased transcript levels across various organs (Supporting Information Figs. S16−S20). These findings suggest a broad and systemic dampening of the inflammatory cytokine network, indicating that EVs$^{GCE-CTM}$ exerts its therapeutic effect at both the transcriptional and protein levels. To further validate the anti-inflammatory efficacy of EVs$^{GCE-CTM}$, we quantified circulating cytokine concentrations using ELISA. Consistently, serum levels of IL1β and IL18 were significantly reduced in EVs$^{GCE-CTM}$–treated mice compared with controls (Fig. 5P and V), confirming that the treatment effectively limits systemic cytokine release. In addition to molecular and serum analyses, cellular responses were evaluated using flow cytometry. Comprehensive flow cytometric analyses across various organs revealed a pronounced decrease in the proportion of CASPASE-1 and PI double-positive cells in the EVs$^{GCE-CTM}$ group (Supporting Information Figs. S21−S25). This reduction reflects decreased pyroptotic cell death and further supports the robust anti-inflammatory activity of EVs$^{GCE-CTM}$ at the cellular level. Collectively, the integration of qPCR, ELISA, and flow cytometry data across multiple tissues highlights the potent inhibition of systemic inflammation by EVs$^{GCE-CTM}$ in septic mice.

In the CLP model, mice underwent 75% cecal ligation, a model associated with high-grade sepsis and 100% mortality[32]. Subsequently, the impact of EVs$^{GCE-CTM}$ on the survival rate of septic mice was assessed. Mice that were operated on using the CLP all died within two days. When injected into the tail vein, EVs^{None} did not show any improvement in the survival of the septic mice (Fig. 6B). Histopathological examination using hematoxylin and eosin staining revealed that EVs$^{GCE-CTM}$ treatment markedly ameliorated organ injury in septic mice. In contrast to the severe tissue damage observed in the CLP and EVs^{None} treated groups, EVs$^{GCE-CTM}$ mitigated cardiomyocyte disorganization and edema, preserved alveolar integrity in the lung, reduced hepatic sinusoidal disruption, and attenuated renal tubular swelling and hemorrhage (Fig. 6A). Comprehensive assessment of cardiac function revealed that sepsis induced by CLP led to significant impairment of both systolic and diastolic performance. Specifically, echocardiographic evaluation showed a marked reduction in ejection fraction and abnormal E/A ratios in septic mice,

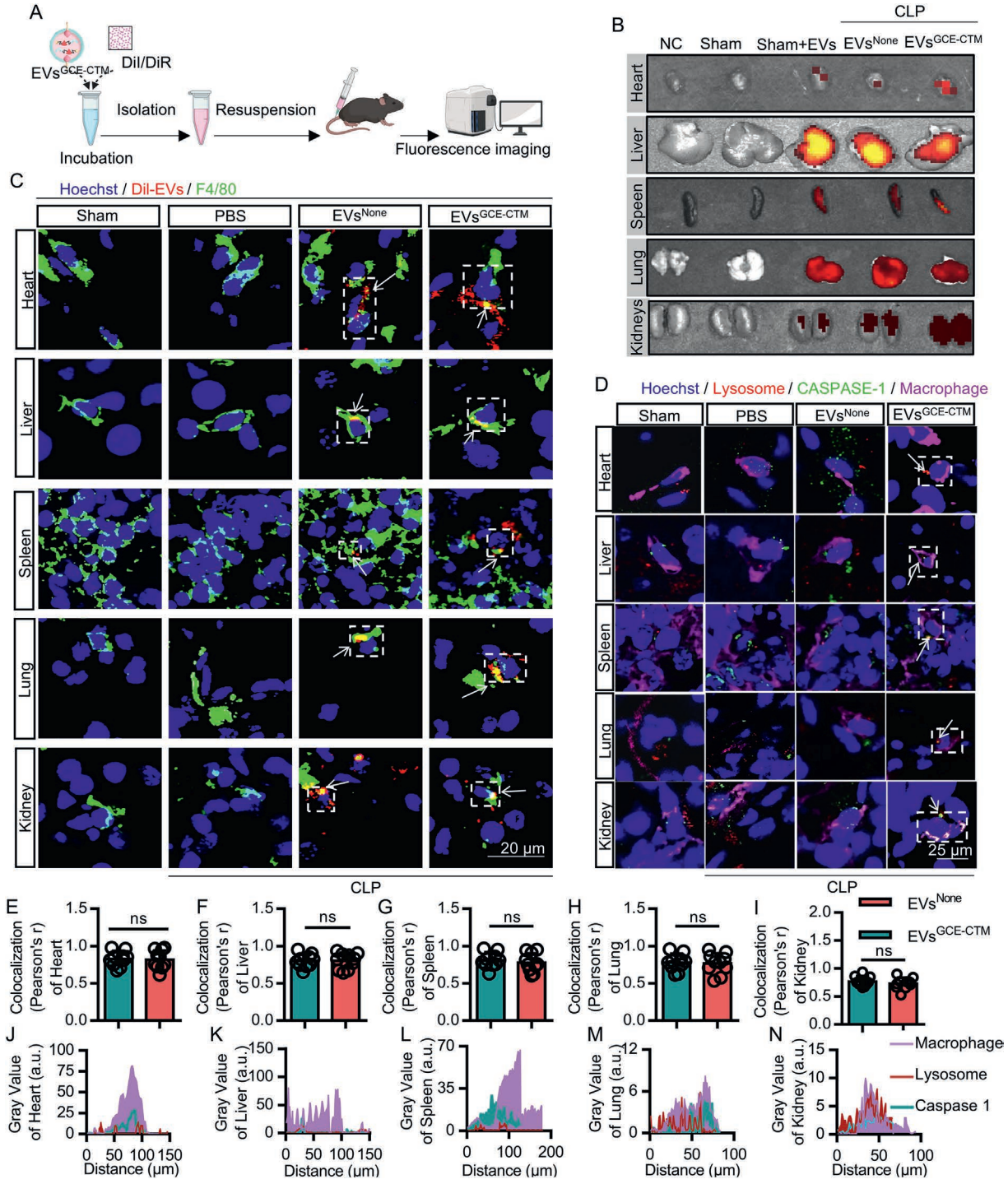

Figure 4 $EVs^{GCE-CTM}$ could be captured by macrophages in septic mice. (A) Schematic diagram of the experimental procedure. Mice were injected with DiR-labeled EVs to monitor *in vivo* distribution. Image created with Biorender.com, with permission. (B) *In vivo* fluorescence imaging analysis of DiR-labeled EVs distribution (4 μg/g) in different organs, including heart, lung, liver, spleen, and kidney ($n = 10$). (C) Representative fluorescence microscopy images of Dil-labeled (red) EVs uptake by macrophages (F4/80, green) in the indicated organs. Nuclei were counterstained with Hoechst (blue). Images are representative of at least three mice. Scale bar = 20 μm. (D) Representative fluorescence microscopy images showing CASPASE-1 localization into lysosomes for degradation in macrophages from the heart, liver, spleen, lung, and kidney of septic mice. EVs^{None} served as the negative control. Scale bar: 25 μm. (E–N) Quantification of fluorescence intensity. Data are presented as mean ± SEM ($n = 10$). ns, not significant by Student's *t*-test.

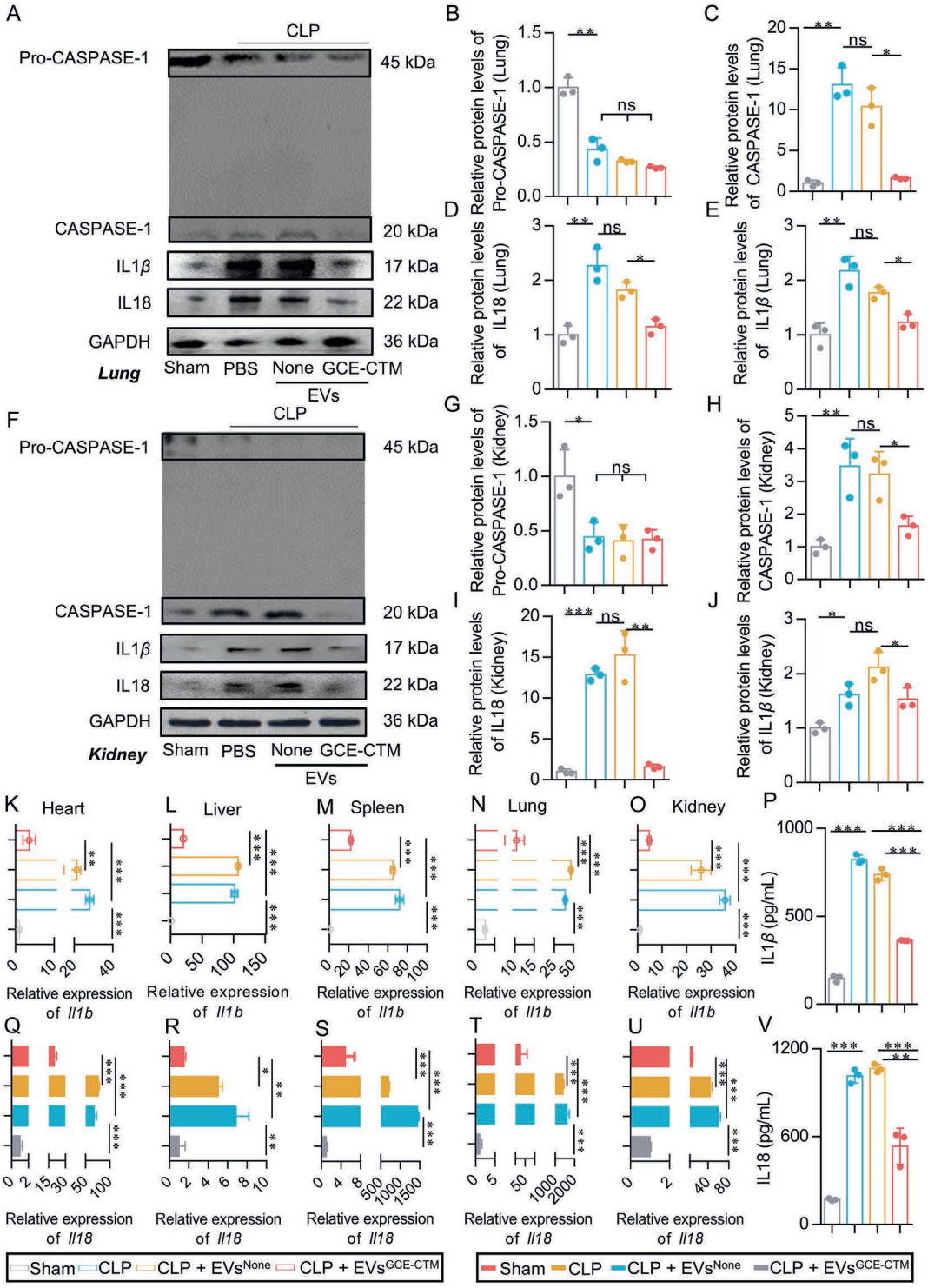

Figure 5 EVs$^{GCE-CTM}$ could effectively alleviate the inflammatory response in septic mice. (A–J) Western blot analysis of Pro-CASPASE-1, cleaved CASPASE-1, IL18, and IL1β expression in different organs (lung and kidney). GAPDH was used as an internal control. Data are presented as the mean ± SEM ($n = 3$). Statistical significance was determined by one-way ANOVA with Tukey's *post hoc* test (ns, not significant; $^*P < 0.05$, $^{**}P < 0.01$, $^{***}P < 0.001$). The qPCR analysis of inflammatory cytokines (*Il18* and *Il1b*) in different organs: heart (K, Q), liver (L, R), spleen (M, S), lung (N, T), and kidney (O, U). GAPDH was used as an internal control. (P, V) ELISA measurement of IL1β and IL18 protein concentrations in blood serum. Data are presented as the mean ± SEM ($n = 3$). Statistical significance was determined by one-way ANOVA with Tukey's *post hoc* test ($^*P < 0.05$, $^{**}P < 0.01$, $^{***}P < 0.001$).

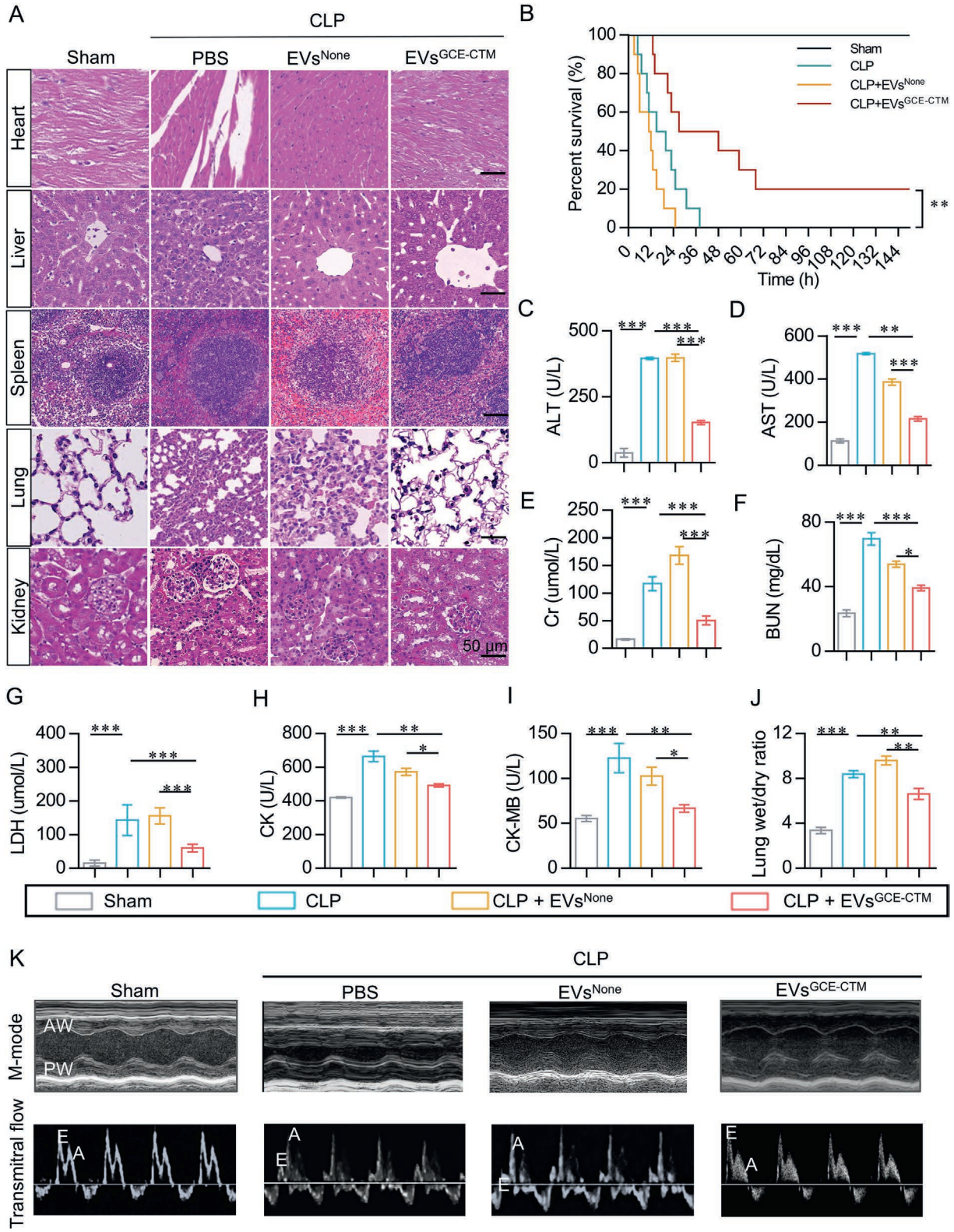

Figure 6 $EVs^{GCE-CTM}$ could effectively alleviate organ injury in septic mice. (A) Representative images of HE-stained sections. Mice received i.v. injections of PBS, EVs^{None}, or $EVs^{GCE-CTM}$ at 6, 12, 18, and 24 h after CLP surgery. Mice receiving the sham operation served as the control group. Images are representative of six mice per group. Scale bar = 50 μm. (B) Survival analysis of mice in the CLP model ($n = 14$). $P < 0.01$ by log-rank test. (C−J) Blood biochemistry analysis demonstrating heart (LDH, CK, CK-MB), liver (ALT, AST), kidney (Cr, BUN) function, and lung (lung wet/dry ratio). Data are presented as the mean ± SEM ($n = 6$). Statistical significance was determined by one-way ANOVA with Tukey's *post hoc* test (*$P < 0.05$, **$P < 0.01$, ***$P < 0.001$). (K) Representative images of M-mode echocardiography and mitral inflow velocity in the indicated groups.

indicating compromised ventricular contractility and relaxation (Fig. 6K). In contrast, treatment with EVs$^{GCE-CTM}$ effectively ameliorated these cardiac dysfunctions, as evidenced by significant improvements in both ejection fraction and E/A ratio (Supporting Information Fig. S26). These findings demonstrate the protective role of EVs$^{GCE-CTM}$ in preserving cardiac function under septic conditions.

In addition to cardiac function, we systematically analyzed a panel of biochemical markers to evaluate injury across multiple organs. Levels of alanine aminotransferase (ALT) and aspartate aminotransferase (AST)—sensitive indicators of hepatic injury—were markedly elevated in the CLP and EVs^{None} groups, reflecting severe liver damage. Similarly, serum creatinine (Cr) and blood urea nitrogen (BUN), which are associated with renal function, were significantly increased, indicating acute kidney injury. Markers of general tissue and myocardial injury, including LDH, creatine kinase (CK), and creatine kinase-muscle/brain (CK-MB), were also substantially elevated in septic mice. Furthermore, the lung wet/dry weight ratio, an established index of pulmonary edema and lung injury, was significantly higher in the CLP group (Fig. 6C–J). Importantly, administration of EVs$^{GCE-CTM}$ markedly reversed these biochemical abnormalities. Mice receiving EVs$^{GCE-CTM}$ exhibited ALT, AST, Cr, BUN, LDH, CK, CK-MB, and wet/dry ratios that approached normal levels, indicating effective protection against multi-organ damage induced by sepsis. These comprehensive results highlight the potent organ-protective effects of EVs$^{GCE-CTM}$ and underscore its therapeutic potential for mitigating sepsis-induced multi-organ dysfunction. Given the high susceptibility of the lungs to sepsis-related injury[33], we conducted a thorough evaluation of pulmonary function to assess the extent of respiratory compromise and the therapeutic impact of EVs$^{GCE-CTM}$. Pulmonary function tests revealed that mice in the CLP and EVs^{None} groups exhibited significant impairments in respiratory mechanics. Specifically, both inspiratory time and expiratory time were markedly prolonged, while tidal volume was significantly reduced compared to healthy controls (Supporting Information Fig. S27). These changes are indicative of restrictive lung disease, which is commonly associated with sepsis-induced acute lung injury and reflects increased lung stiffness and decreased compliance. Importantly, treatment with EVs$^{GCE-CTM}$ led to substantial improvements in these respiratory parameters. Mice receiving EVs$^{GCE-CTM}$ showed normalization of Ti and Te, alongside a restoration of tidal volume toward physiological ranges. This reversal of pulmonary dysfunction suggests that EVs$^{GCE-CTM}$ effectively attenuates sepsis-induced damage to lung tissue, thereby preserving overall respiratory capacity. Additionally, the improvement in lung function was consistent with the observed reduction in pulmonary edema, as evidenced by a decreased wet/dry lung weight ratio in the EVs$^{GCE-CTM}$ group. Taken together, these findings demonstrate that EVs$^{GCE-CTM}$ prevents structural lung injury, underscoring its potential as a therapeutic agent for sepsis-associated lung injury.

Finally, to assess the biosafety profile of our engineered vesicles for systemic administration, we performed hemocompatibility tests. Hemolysis assays confirmed that across all tested concentrations, all EV formulations (EVs^{None}, EVs^{Ctrl}, and EVs$^{GCE-CTM}$) showed hemolysis rates below 2% as calculated by Eq. (1) (Supporting Information Fig. S28), which is well within the ISO 10993-4 safety threshold of <5%.

4. Discussion

This study shows that engineered extracellular vesicles (EVs$^{GCE-CTM}$) that promote lysosomal degradation of CASPASE-1 in macrophages dampen systemic inflammation and improve survival in the murine CLP model of sepsis. Consistent *in vitro* and *in vivo* data demonstrate reduced CASPASE-1 abundance, diminished maturation of IL1β and IL18, and attenuation of multi-organ injury.

Macrophages are central to sepsis pathogenesis, coordinating phagocytosis, antigen presentation, and the production of pro-inflammatory cytokines; CASPASE-1–dependent processing of IL1 family cytokines is a key node in this response[34–37]. Prior approaches to inhibit this axis—including small-molecule inhibitors and nucleic acid–based interventions—have been limited by target specificity, delivery barriers, off-target effects, and, in some cases, target resistance or undruggability of non-enzymatic proteins[38,39]. By leveraging EXPLOR technology to load functional protein complexes into EVs and the natural macrophage tropism of EVs, our platform enables direct post-translational modulation of inflammatory signaling without relying on sustained transcriptional or translational suppression. The observed decreases in CASPASE-1 activity and downstream cytokine maturation align with the central role of pyroptosis and inflammasome signaling in sepsis[40–47].

Despite these promising results, several limitations should be acknowledged. First, our mechanistic analyses focused on macrophages. CASPASE-1 and inflammasome pathways in other myeloid cells, particularly neutrophils, also contribute to sepsis pathophysiology[48–52]. The spatial and temporal dynamics of CASPASE-1 processing and cytokine release in neutrophils under EVs$^{GCE-CTM}$ treatment remain incompletely defined and should be addressed using cell–type–resolved approaches in future work. We also noted a modest exacerbation of select inflammatory readouts in the EVs^{None} group compared with PBS (Fig. 6E and G, Fig. S17C). Although lacking therapeutic cargo, EVs^{None} may retain bioactive components from parental cells. In a primed inflammatory milieu, uptake of such vesicles can deliver non-specific secondary signals, consistent with reports that blank nanocarriers, including native EVs, can act as danger-associated cues[53,54]. Importantly, the marked divergence between EVs^{None} and EVs$^{GCE-CTM}$ supports that the therapeutic effect arises from targeted CASPASE-1 degradation rather than a vehicle effect. Future iterations could incorporate membrane engineering or compositional minimization to reduce innate immune sensing by the control vector.

To position this platform for translation, head-to-head comparisons with established modalities—such as small-molecule CASPASE-1 inhibitors and RNA-based strategies—are needed to delineate relative efficacy, pharmacokinetics, biodistribution, durability, and safety[55,56]. Such benchmarking will clarify whether direct protein degradation affords superior control of hyper-inflammation and more sustained benefit.

Finally, although no overt toxicity was observed in our studies, the long-term fate and potential immunogenicity of engineered EVs require systematic evaluation, particularly with repeated dosing. The use of non-human optogenetic components (CRY2 and CIBN) raises the possibility of adaptive immune responses upon chronic exposure. Future work will focus on evaluating chronic dosing schedules and exploring strategies to enhance biocompatibility to advance the translational potential of this platform.

In summary, these findings support engineered EVs for targeted protein degradation as a viable therapeutic strategy in sepsis. By directly depleting CASPASE-1 in macrophages, $EVs^{GCE-CTM}$ modulate a central inflammatory pathway and improve outcomes in a rigorous preclinical model. The approach is adaptable to other diseases driven by aberrant protein function and warrants further investigation in comparative, long-term preclinical studies and, ultimately, clinical evaluation.

5. Conclusions

In summary, this study elucidates the role of macrophage CASPASE-1 in the maturation of inflammatory cytokines IL18 and IL1β under septic conditions, which in turn amplifies the inflammatory response and contributes to the development of EVs exhibiting intrinsic macrophage-targeting capacity as a drug carrier to sepsis-induced multiple organ failure and mortality. To target this pathway, we established a novel engineered EV system based on an optogenetic strategy designed to promote lysosomal degradation of CASPASE-1. Specifically, PTGFRN−CRY2 and CIBN−GCE−CTM constructs were expressed in HEK293T cells by co-transfection, and blue light irradiation was applied during the production of $EVs^{GCE-CTM}$ to facilitate the packaging of functional components. Functional validation was conducted in an LPS-induced inflammatory model using RAW264.7. Treatment with $EVs^{GCE-CTM}$ resulted in a significant reduction in cellular CASPASE-1 levels, accompanied by decreased expression of IL18 and IL1β, indicating effective suppression of the inflammatory response *in vitro*. Furthermore, in a murine CLP model of sepsis, administration of $EVs^{GCE-CTM}$ significantly improved survival rates, attenuated systemic inflammation, and ameliorated sepsis-associated organ injury. Collectively, these data demonstrate that the $EVs^{GCE-CTM}$ can serve as an effective therapeutic platform to modulate CASPASE-1−mediated inflammation in sepsis, thereby reducing the severity of organ dysfunction and improving overall outcomes.

Acknowledgments

Yuting Du, Dan Xiao and Heng Li contributed equally to this work. This work was in part supported by grants from the National Natural Science Foundation of China (Nos. 82272261, 82402908, and 82101443) and Shaanxi Province Foundation of China (Nos. 2023-CX-PT-02, 2024SF-ZDCYL-03-26, 2021-ZDLSF-03-13, 2021SF-341, 2022SF-025, 2022SF-044, 2024SF-YBXM-115, 2023-YBSF-602, and 2025PT-03).

Author contributions

Yuting Du: Conceptualization, Data Curation, Formal Analysis, Investigation, Methodology, Software, Visualization, Writing-Original Draft, Writing-Review & Editing. Dan Xiao: Data Curation, Funding Acquisition, Visualization, Writing-Review & Editing. Heng Li: Formal Analysis, Writing-Original Draft, Software, Writing-Review & Editing. Li Fan: Conceptualization, Funding Acquisition, Data Curation, Visualization, Writing-Review & Editing. Kuo Shen: Investigation, Formal Analysis. Bin Zhang: Investigation, Visualization. Liang Zhang: Formal Analysis. Lifei Guo: Methodology, Formal Analysis. Qingzhe Li: Visualization, Writing-Original Draft. Jinwang Zheng: Methodology, Writing-Original Draft. Jingxiang Wang: Software, Visualization. Li Yao: Funding Acquisition, Writing-Review & Editing. Guodong Yang: Conceptualization, Funding Acquisition, Formal Analysis, Investigation, Data Curation, Visualization, Writing-Review & Editing. Xuekang Yang: Conceptualization, Data Curation, Formal Analysis, Funding Acquisition, Visualization, Writing-Review & Editing.

Conflicts of interest

The authors declare no conflicts of interest.

Appendix A. Supporting information

Supporting information to this article can be found online at https://doi.org/10.1016/j.apsb.2026.05.007.

References

1. Singer M, Deutschman CS, Seymour CW, Shankar-Hari M, Annane D, Bauer M, et al. The third international consensus definitions for sepsis and septic shock (Sepsis-3). *JAMA* 2016;**315**:801−10.
2. Rudd KE, Johnson SC, Agesa KM, Shackelford KA, Tsoi D, Kievlan DR, et al. Global, regional, and national sepsis incidence and mortality, 1990−2017: analysis for the Global Burden of Disease Study. *Lancet* 2020;**395**:200−11.
3. Levy MM, Fink MP, Marshall JC, Abraham E, Angus D, Cook D, et al. 2001 SCCM/ESICM/ACCP/ATS/SIS international sepsis definitions conference. *Crit Care Med* 2003;**31**:1250−6.
4. Fujii T, Luethi N, Young PJ, Frei DR, Eastwood GM, French CJ, et al. Effect of vitamin C, hydrocortisone, and thiamine *vs* hydrocortisone alone on time alive and free of vasopressor support among patients with septic shock: the VITAMINS randomized clinical trial. *JAMA* 2020;**323**:423−31.
5. Zhang P, Zou B, Liou YC, Huang C. The pathogenesis and diagnosis of sepsis post burn injury. *Burns Trauma* 2021;**9**. tkaa047.
6. Greenhalgh DG. Sepsis in the burn patient: a different problem than sepsis in the general population. *Burns Trauma* 2017;**5**:23.
7. Ouyang Q, Cui J, Wang Y, Liu K, Zhan Y, Zhuo W, et al. eIF3a function in immunity and protection against severe sepsis by regulating B cell quantity and function through m6A modification. *Acta Pharm Sin B* 2025;**15**:1571−88.
8. Li D, Wei R, Zhang X, Gong S, Wan M, Wang F, et al. Gut commensal metabolite rhamnose promotes macrophages phagocytosis by activating SLC12A4 and protects against sepsis in mice. *Acta Pharm Sin B* 2024;**14**:3068−85.
9. Fang D, Li Y, He B, Gu D, Zhang M, Guo J, et al. Gastrin attenuates sepsis-induced myocardial dysfunction by down-regulation of TLR4 expression in macrophages. *Acta Pharm Sin B* 2023;**13**:3756−69.
10. van der Poll T, Shankar Hari M, Wiersinga WJ. The immunology of sepsis. *Immunity* 2021;**54**:2450−64.
11. Tschernatsch M, Juenemann M, Alhaidar F, El Shazly J, Butz M, Meyer M, et al. Epileptic seizure discharges in patients after open chamber cardiac surgery-a prospective prevalence pilot study using continuous electroencephalography. *Intensive Care Med* 2020;**46**: 1418−24.
12. Wang H, Hong LJ, Huang JY, Jiang Q, Tao RR, Tan C, et al. P2RX7 sensitizes Mac-1/ICAM-1-dependent leukocyte-endothelial adhesion and promotes neurovascular injury during septic encephalopathy. *Cell Res* 2015;**25**:674−90.
13. Giamarellos-Bourboulis EJ, van de Veerdonk FL, Mouktaroudi M, Raftogiannis M, Antonopoulou A, Joosten LAB, et al. Inhibition of CASPASE-1 activation in Gram-negative sepsis and experimental endotoxemia. *Crit Care* 2011;**15**:R27.
14. Matute-Bello G. Targeting CASPASE-1 in sepsis: a novel approach to an old problem. *Intensive Care Med* 2007;**33**:755−7.

15. Marei H, Tsai W-TK, Kee Y-S, Ruiz K, He J, Cox C, et al. Antibody targeting of E3 ubiquitin ligases for receptor degradation. *Nature* 2022;**610**:182−9.
16. Sakamoto KM, Kim KB, Kumagai A, Mercurio F, Crews CM, Deshaies RJ. Protacs: chimeric molecules that target proteins to the Skp1−Cullin-F box complex for ubiquitination and degradation. *Proc Natl Acad Sci U S A* 2001;**98**:8554−9.
17. Li Q, Wang P, Ye K, Cai H. Central role of SIAH inhibition in DCC-dependent cardioprotection provoked by netrin-1/NO. *Proc Natl Acad Sci U S A* 2015;**112**:899−904.
18. Li K, Crews CM. PROTACs: past, present and future. *Chem Soc Rev* 2022;**51**:5214−36.
19. Wang M, Zhao X, Cui Y, Gui H, Wang S, Liu Z, et al. Extracellular vesicles in burn injury: roles, mechanisms, and applications. *Burns Trauma* 2025;**13**. tkaf006.
20. Li Z, Zhou X, Gao X, Bai D, Dong Y, Sun W, et al. Fusion protein engineered exosomes for targeted degradation of specific RNAs in lysosomes: a proof-of-concept study. *J Extracell Vesicles* 2020;**9**:1816710.
21. Choi H, Kim Y, Mirzaaghasi A, Heo J, Kim YN, Shin JH, et al. Exosome-based delivery of super-repressor I$\kappa B\alpha$ relieves sepsis-associated organ damage and mortality. *Sci Adv* 2020;**6**. eaaz6980.
22. Liu Z, Wang C, Yang J, Chen Y, Zhou B, Abbott DW, et al. CASPASE-1 engages full-length Gasdermin D through two distinct interfaces that mediate CASPASE recruitment and substrate cleavage. *Immunity* 2020;**53**:106−14.e5.
23. Fan X, Jin WY, Lu J, Wang J, Wang YT. Rapid and reversible knockdown of endogenous proteins by peptide-directed lysosomal degradation. *Nat Neurosci* 2014;**17**:471−80.
24. Yim N, Ryu S-W, Choi K, Lee KR, Lee S, Choi H, et al. Exosome engineering for efficient intracellular delivery of soluble proteins using optically reversible protein-protein interaction module. *Nat Commun* 2016;**7**:12277.
25. Hernández-Candia CN, Pearce S, Tucker CL. A modular tool to query and inducibly disrupt biomolecular condensates. *Nat Commun* 2021; **12**:1809.
26. Fan L, Yao L, Li Z, Wan Z, Sun W, Qiu S, et al. Exosome-based mitochondrial delivery of circRNA mSCAR alleviates sepsis by orchestrating macrophage activation. *Adv Sci (Weinh)* 2023;**10**: e2205692.
27. Huang B, Qian Y, Xie S, Ye X, Chen H, Chen Z, et al. Ticagrelor inhibits the NLRP3 inflammasome to protect against inflammatory disease independent of the P2Y12 signaling pathway. *Cell Mol Immunol* 2021;**18**:1278−89.
28. Hooftman A, Angiari S, Hester S, Corcoran SE, Runtsch MC, Ling C, et al. The Immunomodulatory metabolite itaconate modifies NLRP3 and inhibits inflammasome activation. *Cell Metab* 2020;**32**:468−78.e7.
29. Wang M, Wu M, Liu X, Shao S, Huang J, Liu B, et al. Pyroptosis remodeling tumor microenvironment to enhance pancreatic cancer immunotherapy driven by membrane anchoring photosensitizer. *Adv Sci (Weinh)* 2022;**9**:e2202914.
30. Rittirsch D, Huber-Lang MS, Flierl MA, Ward PA. Immunodesign of experimental sepsis by cecal ligation and puncture. *Nat Protoc* 2009;**4**: 31−6.
31. Kaffe E, Fiorotto R, Pellegrino F, Mariotti V, Amenduni M, Cadamuro M, et al. β-Catenin and interleukin-1β-dependent chemokine (C−X−C motif) ligand 10 production drives progression of disease in a mouse model of congenital hepatic fibrosis. *Hepatology* 2018;**67**:1903−19.
32. Liu Y, Song R, Zhao L, Lu Z, Li Y, Zhan X, et al. m^{6}A demethylase ALKBH5 is required for antibacterial innate defense by intrinsic motivation of neutrophil migration. *Signal Transduct Targeted Ther* 2022;**7**:194.
33. Shen K, Wang X, Wang Y, Jia Y, Zhang Y, Wang K, et al. miR-125b-5p in adipose derived stem cells exosome alleviates pulmonary microvascular endothelial cells ferroptosis *via* Keap1/Nrf2/GPX4 in sepsis lung injury. *Redox Biol* 2023;**62**:102655.
34. Zhang YY, Ning BT. Signaling pathways and intervention therapies in sepsis. *Signal Transduct Targeted Ther* 2021;**6**:407.
35. Yuan Y, Fan G, Liu Y, Liu L, Zhang T, Liu P, et al. The transcription factor KLF14 regulates macrophage glycolysis and immune function by inhibiting HK2 in sepsis. *Cell Mol Immunol* 2022;**19**:504−15.
36. Houtman J, Freitag K, Gimber N, Schmoranzer J, Heppner FL, Jendrach M. Beclin1-driven autophagy modulates the inflammatory response of microglia *via* NLRP3. *EMBO J* 2019;**38**:e99430.
37. Stearns-Kurosawa DJ, Osuchowski MF, Valentine C, Kurosawa S, Remick DG. The pathogenesis of sepsis. *Annu Rev Pathol* 2011;**6**: 19−48.
38. Xie X, Yu T, Li X, Zhang N, Foster LJ, Peng C, et al. Recent advances in targeting the "undruggable" proteins: from drug discovery to clinical trials. *Signal Transduct Targeted Ther* 2023;**8**:335.
39. Barrangou R, Birmingham A, Wiemann S, Beijersbergen RL, Hornung V, Smith A van B. Advances in CRISPR-Cas9 genome engineering: lessons learned from RNA interference. *Nucleic Acids Res* 2015;**43**:3407−19.
40. Wei X, Xie F, Zhou X, Wu Y, Yan H, Liu T, et al. Role of pyroptosis in inflammation and cancer. *Cell Mol Immunol* 2022;**19**:971−92.
41. Zhang N, Zhang J, Yang Y, Shan H, Hou S, Fang H, et al. A palmitoylation-depalmitoylation relay spatiotemporally controls GSDMD activation in pyroptosis. *Nat Cell Biol* 2024;**26**:757−69.
42. Liu Y, Lei H, Zhang W, Xing Q, Liu R, Wu S, et al. Pyroptosis in renal inflammation and fibrosis: current knowledge and clinical significance. *Cell Death Dis* 2023;**14**:472.
43. Yu P, Zhang X, Liu N, Tang L, Peng C, Chen X. Pyroptosis: mechanisms and diseases. *Signal Transduct Targeted Ther* 2021;**6**:128.
44. Shi J, Zhao Y, Wang K, Shi X, Wang Y, Huang H, et al. Cleavage of GSDMD by inflammatory CASPASEs determines pyroptotic cell death. *Nature* 2015;**526**:660−5.
45. He Wt, Wan H, Hu L, Chen P, Wang X, Huang Z, et al. Gasdermin D is an executor of pyroptosis and required for interleukin-1β secretion. *Cell Res* 2015;**25**:1285−98.
46. Liu Y, Pan R, Ouyang Y, Gu W, Xiao T, Yang H, et al. Pyroptosis in health and disease: mechanisms, regulation and clinical perspective. *Signal Transduct Targeted Ther* 2024;**9**:245.
47. Kayagaki N, Webster JD, Newton K. Control of cell death in health and disease. *Annu Rev Pathol* 2024;**19**:157−80.
48. Gollomp K, Sarkar A, Harikumar S, Seeholzer SH, Arepally GM, Hudock K, et al. Fc-modified HIT-like monoclonal antibody as a novel treatment for sepsis. *Blood* 2020;**135**:743−54.
49. Etulain J, Martinod K, Wong SL, Cifuni SM, Schattner M, Wagner DD. P-selectin promotes neutrophil extracellular trap formation in mice. *Blood* 2015;**126**:242−6.
50. Abasıyanık MF, Wolfe K, Van Phan H, Lin J, Laxman B, White SR, et al. Ultrasensitive digital quantification of cytokines and bacteria predicts septic shock outcomes. *Nat Commun* 2020;**11**:2607.
51. Tidball JG. Inflammatory cell response to acute muscle injury. *Med Sci Sports Exerc* 1995;**27**:1022−32.
52. Keitelman IA, Shiromizu CM, Zgajnar NR, Danielián S, Jancic CC, Martí MA, et al. The interplay between serine proteases and CASPASE-1 regulates the autophagy-mediated secretion of interleukin-1 beta in human neutrophils. *Front Immunol* 2022;**13**:832306.
53. Danesh A, Inglis HC, Jackman RP, Wu S, Deng X, Muench MO, et al. Exosomes from red blood cell units bind to monocytes and induce proinflammatory cytokines, boosting T-cell responses *in vitro*. *Blood* 2013;**123**:687−96.
54. Buzas EI. The roles of extracellular vesicles in the immune system. *Nat Rev Immunol* 2022;**23**:236−50.
55. Zhu X, Xu K, Ai S, Zhang Y, Chu C, Wei R, et al. miR-126-5p protects from URSA *via* inhibiting CASPASE-1-dependent pyroptosis of trophoblast cells. *Cell Mol Life Sci* 2025;**82**:204.
56. Xi H, Zhang Y, Xu Y, Yang WY, Jiang X, Sha X, et al. CASPASE-1 inflammasome activation mediates homocysteine-induced pyroptosis in endothelial cells. *Circ Res* 2016;**118**:1525−39.